

Wavelength-Tunable First-Order Narrowband Fiber Comb Filter Incorporating All-Quarter-Wave Polarization Transformation

Jaehoon Jung ^{1b} and Yong Wook Lee ^{1b}

Abstract—In this article, we propose a wavelength-tunable first-order narrowband fiber comb filter that incorporates all-quarter-wave polarization transformation. The proposed filter is composed of a polarization beam splitter to form a polarization-diversified fiber loop, two equally long polarization-maintaining fiber segments, and four quarter-wave plates to modify the absolute phase of the narrowband transmittance of the filter. The transmittance function of the filter was found theoretically utilizing the Jones matrix formulation. Based on this filter transmittance, we derived the azimuthal angles (AAs) of the waveplates, which can tune the spectral wavelength of the filter by continuously adjusting the transmittance phase. Narrowband comb spectra calculated at some selected sets of these four waveplate AAs showed sequential wavelength changes. In particular, the calculation result was experimentally validated.

Index Terms—Fiber optic components, comb filters, polarization, wavelength tuning, narrowband.

I. INTRODUCTION

OPTICAL fiber comb filters have garnered much interest in a variety of fields, including optical sensors [1], [2], microwave photonic filters [3], [4], and optical networks [5], [6], owing to their compact dimensions, seamless integration capability, and compatibility with established fiber-optic systems. They provide an efficient means of passing or blocking selective wavelength components in optical signals. In particular, the wavelength tuning capability of their passbands or stopbands offers precise manipulation of specific spectral components, thereby facilitating diverse functionalities in optical signal processing. Several techniques have been proposed to achieve wavelength tunability in comb filters. These techniques

include a Mach-Zehnder interferometer [7], [8], [9], [10], a Sagnac birefringence interferometer [11], [12], a polarization-interference-based ring cavity [13], a hybrid fiber structure based on a few-mode fiber core-offset-spliced with single-mode fiber (SMF) [14], and a polarization-diversified loop structure (PDLs) [15], [16]. Among the various comb filters, PDLs-based comb filters are more efficient than other comb filters in terms of wavelength switching or tuning of comb spectra [15], [16] and generation of higher-order comb spectra [17], [18]. Wavelength tunability in zeroth-order PDLs comb filters has been achieved theoretically and experimentally in 2017 by incorporating three types of ordered waveplate combinations, such as a set of a half-wave plate (HWP) and a quarter-wave plate (QWP), a set of a QWP and an HWP, and two QWPs [19], [20]. Even in the case of first-order PDLs comb filters, the wavelength tunability of flat-top [21], [22], [23] and narrowband [24], [25], [26] comb spectra has been explored until recently using composite waveplate combinations of HWPs and QWPs. However, because it is relatively complex to convert a given input state of polarization (SOP) to the desired output SOP utilizing two QWPs instead of heterogeneous combinations of a QWP and an HWP, there has been no study of a wavelength-tunable narrowband PDLs comb filter employing polarization controllers homogeneously comprised of QWPs. This SOP conversion complexity is attributed to the fact that the output SOP (SOP_{out}) of a QWP follows a more complicated path on the Poincaré sphere than the SOP_{out} of an HWP, while the azimuthal angle (AA) of the waveplate varies by 180° . The use of multiple QWPs made from the same quarter-wavelength birefringent media can enhance manufacturing efficiency and reduce device footprint, particularly when integrating the filter into other optical systems. This shift from HWPs to QWPs as polarization controllers can also lead to improvements in form factor, resulting in a reduction in overall system volume and weight. It also provides greater flexibility in system design. Here, we propose a continuously wavelength-tunable narrowband PDLs comb filter based on all-quarter-wave polarization transformation, that is, employing polarization controllers composed only of QWPs. The proposed comb filter comprises a polarization beam splitter (PBS) to construct the PDLs, two polarization-maintaining fiber (PMF) segments of the same length, and two polarization controllers placed in front of each PMF. The second PMF segment, located between the second polarization controller and the PBS, was

Manuscript received 28 December 2023; revised 11 April 2024; accepted 16 April 2024. Date of publication 24 April 2024; date of current version 8 May 2024. This work was supported by the National Research Foundation of Korea (NRF) through Basic Science Research Program funded by the Ministry of Education under Grant 2019R1I1A3A01046232. (Corresponding author: Yong Wook Lee.)

Jaehoon Jung is with the Department of Electronics and Electrical Engineering, Dankook University, Yongin 16890, South Korea (e-mail: andyjung@dku.edu).

Yong Wook Lee is with the School of Electrical Engineering, Pukyong National University, Busan 48513, South Korea, and also with the Industry 4.0 Convergence Bionics Engineering, Pukyong National University, Busan 48513, South Korea (e-mail: yongwook@pknu.ac.kr).

This article has supplementary downloadable material available at <https://doi.org/10.1109/JPHOT.2024.3393147>, provided by the authors.

Digital Object Identifier 10.1109/JPHOT.2024.3393147

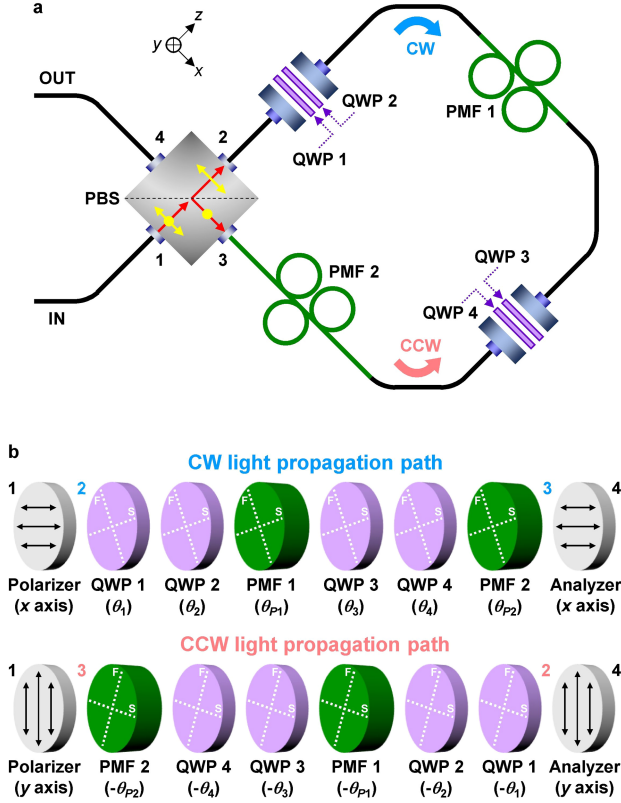


Fig. 1. (a) Schematic diagram of proposed filter and (b) light propagation paths of CW and CCW rotation components.

butt-coupled to the PBS so that its slow axis was oriented at an angle of 22.5° relative to the horizontal axis of the PBS. First, the transmittance function of the proposed filter was derived theoretically using the Jones matrix formulation. Based on this transmittance function, we identified the AA sets of the four QWPs that allow the phase ψ of the narrowband transmittance function, which can be obtained in the classical fan-type Solc filter, to vary from 1° to 360° with increments of 1° . An increase of 360° in ψ results in a wavelength shift of one fringe period, i.e., a free spectral range λ_{FSR} , in the narrowband comb spectrum. We then confirmed that the narrowband comb spectra calculated at the identified waveplate AA sets shifted to a longer wavelength region with increasing ψ . Finally, this theoretical analysis was experimentally demonstrated.

II. PRINCIPLES OF OPERATION

Fig. 1(a) shows a schematic diagram of the proposed narrowband comb filter. A four-port SMF-pigtailed PBS forms a polarization-diversified loop by connecting its two ports, namely ports 2 and 3. This loop contains two polarization controllers and two PMF segments (denoted PMF 1 and PMF 2), with each polarization controller placed before each PMF. Each polarization controller consists of two QWPs, and the two QWPs before PMF 1 are labeled QWP 1 and QWP 2, while those before PMF 2 are labeled QWP 3 and QWP 4. The second PMF segment, PMF 2, is directly connected to port 3 of the PBS by butt coupling so that its slow axis should be aligned at 22.5° relative to the horizontal axis of the PBS. The input light entering port 1 of the

PBS is decomposed into linear horizontal polarization (LHP) and linear vertical polarization (LVP) components coming out of ports 2 and 3 of the PBS, respectively. For simplicity, we assume that the horizontal and vertical axes of the PBS are the x and y axes, respectively. These LHP (x polarization) and LVP (y polarization) components pass through other optical components in the filter, rotating clockwise (CW) and counter-clockwise (CCW), respectively. The optical components viewed by the CW and CCW rotation components are shown in Fig. 1(b) along two optical paths, referred to as the CW and CCW light propagation paths, respectively. Along the CW light propagation path, the x -polarization component sequentially goes through QWP 1, QWP 2, PMF 1, QWP 3, QWP 4, and PMF 2, whose slow-axis AAs are θ_1 , θ_2 , θ_{P1} , θ_3 , θ_4 , and θ_{P2} , respectively. In the case of the CCW path, the y -polarization component propagates through PMF 2, QWP 4, QWP 3, PMF 1, QWP 2, and QWP 1, whose slow-axis AAs are $-\theta_{P2}$, $-\theta_4$, $-\theta_3$, $-\theta_{P1}$, $-\theta_2$, and $-\theta_1$, respectively, in the reverse order to the CW path. The x - and y -polarization components passing through PMF 2 and QWP 1 eventually undergo x and y polarizers, respectively, when they exit port 4 of the PBS. The PMFs, as birefringent elements sandwiched between two linear polarizers, produce polarization interference resulting in a comb spectrum. The free spectral range λ_{FSR} of this interference spectrum is determined by the phase retardation difference Γ ($= 2\pi BL/\lambda$) of each PMF, where B , L , and λ are the PMF birefringence, PMF length, and free-space wavelength, respectively [27]. In both the CW and CCW paths, an interference spectrum with the same λ_{FSR} is generated by polarization interference, but the insertion losses of these two spectra are different depending on the input polarization of the filter [15]. Because the above two interference spectra, whose SOPs are LHP and LVP, are orthogonally polarized, the arithmetic sum of these two spectra can be used to obtain the output spectrum of the filter. Since an arbitrary SOP can always be synthesized from the two bases of LHP and LVP, the output spectrum is independent of the input polarization [15]. While λ_{FSR} is slightly varied by a change in Γ , the spectral position of the interference spectrum is also modified. An increase of 360° in the original phase retardation difference Γ , which can be realized by placing some waveplates before PMFs and adjusting their AAs, causes a redshift of the fringe spectrum by λ_{FSR} . Regarding our comb filter, two QWPs located in front of each PMF can add the extra phase retardation difference to the original phase retardation difference generated by each PMF, and finally tune the wavelength of the comb spectrum created by the PMFs.

Considering the light propagation along the CW and CCW paths within the filter, the transfer matrix T of the filter can be expressed as (1) using the Jones matrix formulation [28].

$$\begin{aligned}
 T = & \begin{bmatrix} 1 & 0 \\ 0 & 0 \end{bmatrix} T_{P2}(\theta_{P2}) T_{Q4}(\theta_4) T_{Q3}(\theta_3) \\
 & \times T_{P1}(\theta_{P1}) T_{Q2}(\theta_2) T_{Q1}(\theta_1) \begin{bmatrix} 1 & 0 \\ 0 & 0 \end{bmatrix} \\
 & + \begin{bmatrix} 0 & 0 \\ 0 & 1 \end{bmatrix} T_{Q1}(-\theta_1) T_{Q2}(-\theta_2) T_{P1}(-\theta_{P1})
 \end{aligned}$$

$$\times T_{Q3}(-\theta_3) T_{Q4}(-\theta_4) T_{P2}(-\theta_{P2}) \begin{bmatrix} 0 & 0 \\ 0 & 1 \end{bmatrix}, \quad (1)$$

where $T_{Q1}, T_{Q2}, T_{Q3}, T_{Q4}, T_{P1}$, and T_{P2} are the Jones transfer matrices of QWP 1, QWP 2, QWP 3, QWP 4, PMF 1, and PMF 2, respectively. Also, $\theta_1, \theta_2, \theta_3, \theta_4, \theta_{P1}$, and $\theta_{P2} (= 22.5^\circ)$ are their corresponding slow-axis AAs. From this transfer matrix T , the filter transmittance t_f can be derived and is given by (2).

$$t_f = \frac{1}{2} [2a_0^2 + a_1^2 + a_2^2 + 2b_0^2 + b_1^2 + b_2^2] + 2(a_0a_1 + b_0b_1) \cos \Gamma + 2(a_0a_2 + b_0b_2) \sin \Gamma + \left(\frac{a_1^2 - a_2^2 + b_1^2 - b_2^2}{2} \right) \cos 2\Gamma + (a_1a_2 + b_1b_2) \sin 2\Gamma, \quad (2)$$

where $a_0 = -\sin(\theta_1 - \theta_2)\sin(\theta_3 - \theta_4)\cos(\theta_1 - \theta_2 + \theta_{P1} - \theta_{P2})\cos(\theta_3 - \theta_4 - \theta_{P1} + \theta_{P2}) - \cos(\theta_1 - \theta_2)\cos(\theta_3 - \theta_4)\sin(\theta_1 + \theta_2 - \theta_{P1} - \theta_{P2})\sin(\theta_3 + \theta_4 - \theta_{P1} - \theta_{P2})$, $a_1 = \sin(\theta_1 - \theta_2)\sin(\theta_3 - \theta_4)\sin(\theta_1 - \theta_2 + \theta_{P1} - \theta_{P2})\sin(\theta_3 - \theta_4 - \theta_{P1} + \theta_{P2}) - \cos(\theta_1 - \theta_2)\cos(\theta_3 - \theta_4)\cos(\theta_1 + \theta_2 - \theta_{P1} - \theta_{P2})\cos(\theta_3 + \theta_4 - \theta_{P1} - \theta_{P2})$, $a_2 = -\sin(\theta_1 - \theta_2)\cos(\theta_3 - \theta_4)\sin(\theta_1 - \theta_2 + \theta_{P1} - \theta_{P2})\cos(\theta_3 + \theta_4 - \theta_{P1} - \theta_{P2}) - \cos(\theta_1 - \theta_2)\sin(\theta_3 - \theta_4)\cos(\theta_1 + \theta_2 - \theta_{P1} - \theta_{P2})\sin(\theta_3 - \theta_4 - \theta_{P1} + \theta_{P2})$, $b_0 = \cos(\theta_1 - \theta_2)\sin(\theta_3 - \theta_4)\sin(\theta_1 + \theta_2 - \theta_{P1} + \theta_{P2})\cos(\theta_3 - \theta_4 - \theta_{P1} + \theta_{P2}) - \sin(\theta_1 - \theta_2)\cos(\theta_3 - \theta_4)\cos(\theta_1 - \theta_2 + \theta_{P1} + \theta_{P2})\sin(\theta_3 + \theta_4 - \theta_{P1} - \theta_{P2})$, $b_1 = -\cos(\theta_1 - \theta_2)\sin(\theta_3 - \theta_4)\cos(\theta_1 + \theta_2 - \theta_{P1} + \theta_{P2})\sin(\theta_3 - \theta_4 - \theta_{P1} + \theta_{P2}) - \sin(\theta_1 - \theta_2)\cos(\theta_3 - \theta_4)\sin(\theta_1 - \theta_2 + \theta_{P1} + \theta_{P2})\cos(\theta_3 + \theta_4 - \theta_{P1} - \theta_{P2})$, and $b_2 = \cos(\theta_1 - \theta_2)\cos(\theta_3 - \theta_4)\cos(\theta_1 + \theta_2 - \theta_{P1} + \theta_{P2})\cos(\theta_3 + \theta_4 - \theta_{P1} - \theta_{P2}) - \sin(\theta_1 - \theta_2)\sin(\theta_3 - \theta_4)\sin(\theta_1 - \theta_2 + \theta_{P1} + \theta_{P2})\sin(\theta_3 - \theta_4 - \theta_{P1} + \theta_{P2})$. The mathematical formulation assumes that the insertion losses of all optical components within the filter are zero and that the phase retardation differences of all QWPs are independent of wavelength over a wavelength range of interest. A narrowband transmittance of a comb spectrum can be obtained using a conventional fan-type Solc filter with two birefringence elements [27]. Because the proposed filter also has two birefringence elements between polarizing elements, it can achieve narrowband transmittance by properly controlling the AAs of the four QWPs due to structural similarity. These QWPs also induce an additional phase retardation difference ψ to the original phase retardation difference Γ established by each PMF, thereby changing the phase of the narrowband transmittance by ψ . Thus, the narrowband transmittance function t_{narrow} that can be realized in the proposed filter is given by (3).

$$t_{\text{narrow}} = \frac{3}{8} + \frac{1}{2} \cos(\Gamma + \psi) + \frac{1}{8} \cos 2(\Gamma + \psi). \quad (3)$$

From the above expression of t_{narrow} , we can directly expect the wavelength tunability of the narrowband comb spectrum mediated by modifying ψ , since the transmittance phase ψ defines the wavelength position of the comb spectrum.

Fig. 2 shows 360 sets of the four waveplate AAs ($\theta_1, \theta_2, \theta_3, \theta_4$) plotted according to the transmittance phase ψ , which changes from 1° to 360° in steps of 1° . The above QWP AA sets were theoretically derived from the direct comparison between

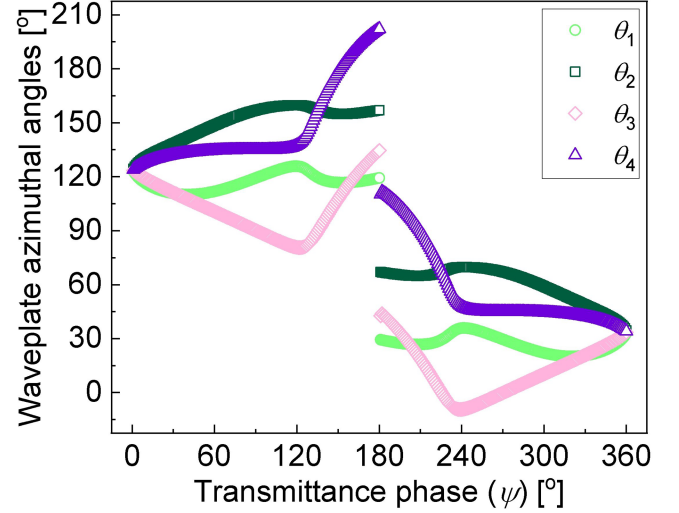


Fig. 2. Variations of four waveplate AAs ($\theta_1, \theta_2, \theta_3, \theta_4$) according to ψ changing from 1° to 360° in increments of 1° .

(2) and (3) with ψ fixed at one of the 360 values (1° to 360°) and θ_{P1} set to 0° . A particular value of ψ from 1° to 360° is associated with a set of ($\theta_1, \theta_2, \theta_3, \theta_4$) in one-to-one correspondence. The four QWP AAs as functions of ψ , namely $\theta_1(\psi), \theta_2(\psi), \theta_3(\psi)$, and $\theta_4(\psi)$, are indicated by green circles, olive squares, pink diamonds, and purple triangles, respectively. Since $\theta_1(\psi), \theta_2(\psi), \theta_3(\psi)$, and $\theta_4(\psi)$ are all QWP AAs, they have an angular periodicity of 180° . Although each AA trace cannot be represented as a simple explicit function of ψ , it has a contiguous sequence of AA values for the entire ψ range. This implies that we can implement a wavelength tuning of one free spectral range (here 0.8 nm) in the comb spectrum of t_{narrow} by sequentially selecting ($\theta_1, \theta_2, \theta_3, \theta_4$) along these four traces so that ψ is tuned from 1° to 360° . In other words, the appropriate choice of ($\theta_1, \theta_2, \theta_3, \theta_4$) from the 360 sets of the four QWP AAs shown in Fig. 2 enables the absolute phase tuning of t_{narrow} , which results in the wavelength tuning of the narrowband comb spectrum. Further calculations also confirmed that the four AA traces $\theta_1(\psi), \theta_2(\psi), \theta_3(\psi)$, and $\theta_4(\psi)$ show the same trajectories even for ψ values with smaller angular steps ($< 1^\circ$).

In order to delve deeper into the relationship among the four QWP AA traces depicted in Fig. 2, we selected two out of the four traces, namely $\theta_1(\psi)$ and $\theta_2(\psi)$, or $\theta_3(\psi)$ and $\theta_4(\psi)$, and closely examined a parametric curve generated by these chosen traces, which play the role of parametric equations where ψ acts as the parameter. When ψ increases from 1° to 360° with a step of 1° , the parametric equations for $\theta_1(\psi)$ and $\theta_2(\psi)$ define the parametric curve shown in Fig. 3(a). Illustrated in Fig. 3(b) is a three-dimensional representation of the parametric curve of θ_1 and θ_2 , showcasing how the curve varies with ψ in the Cartesian coordinate system of ψ, θ_1 , and θ_2 . When this three-dimensional curve is projected onto the θ_1 - θ_2 plane, it translates into the parametric curve shown in Fig. 3(a), which is composed of two C-shaped traces. Two curved thread-like trajectories, located at the top right and bottom left when viewed in the θ_1 - θ_2 plane of Fig. 3(b), are defined for ψ values ranging

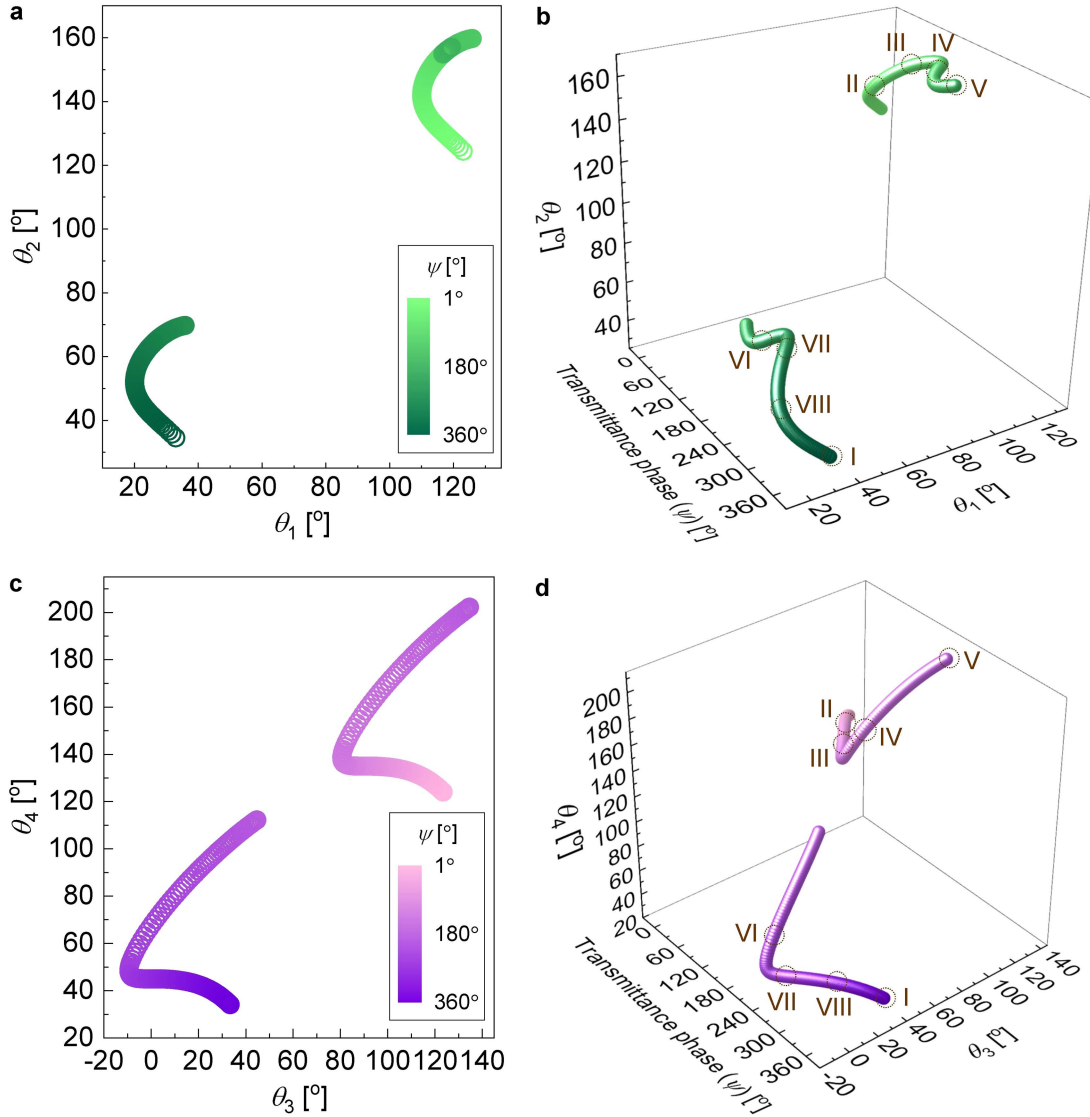


Fig. 3. (a) Parametric curve defined by parametric equations for $\theta_1(\psi)$ and $\theta_2(\psi)$ and (b) its three-dimensional representation in Cartesian coordinate system of ψ , θ_1 , and θ_2 . (c) Parametric curve defined by parametric equations for $\theta_3(\psi)$ and $\theta_4(\psi)$ and (d) its 3D representation in Cartesian coordinate system of ψ , θ_3 , and θ_4 . Here, ψ changes from 1° to 360° with a step of 1° .

from 1° to 180° and from 181° to 360° , respectively. It is clear from Fig. 3(b) that a point (θ_1, θ_2) on the curve of Fig. 3(a) retraces the curve several times as ψ changes in a ψ range from 81° to 280° . Thus, it is possible for a certain AA point to have two or more ψ values, i.e., multiple parameters, within the ψ range above. Outside the ψ range where AA points on the parametric curve in Fig. 3(a) have multiple parameters, the AA points on the C-shaped traces at the top right and bottom left move in a clockwise and counterclockwise direction, respectively, as ψ increases. Likewise, as ψ increases from 1° to 360° with a step of 1° , the parametric equations for $\theta_3(\psi)$ and $\theta_4(\psi)$ determine the parametric curve shown in Fig. 3(d), and this parametric curve can be visualized in 3D in the Cartesian coordinate system of ψ , θ_3 , and θ_4 , as shown in Fig. 3(d). The projection of the 3D curve in Fig. 3(d) onto the θ_3 - θ_4 plane becomes the parametric curve of θ_3 and θ_4 in Fig. 3(c), which appears as inequality symbols. Similar to the curve in Fig. 3(b), two 3D trajectories, located at

the top right and bottom left when viewed in the θ_3 - θ_4 plane of Fig. 3(d), are defined for ψ values ranging from 1° to 180° and from 181° to 360° , respectively. Unlike the parametric curve of θ_1 and θ_2 , a point (θ_3, θ_4) on the parametric curve of θ_3 and θ_4 does not have multiple parameters, but exhibits a consistent and unidirectional movement from bottom to top and from top to bottom along the curve for the upper and lower trajectories, respectively, as ψ increases. The deterministic trajectories in Fig. 3, which are singular in the proposed filter, can expedite the prediction of QWP AAs for continuous wavelength tuning of narrowband comb spectra. For the AA trajectories in Fig. 3(b) and (d), the greenish and purplish circles denoted by I, II, III, IV, V, VI, VII, and VIII indicate the eight selected AA sets of (θ_1, θ_2) and (θ_3, θ_4) for the discrete wavelength shift of the narrowband comb spectrum, respectively. At these eight AA sets of $(\theta_1, \theta_2, \theta_3, \theta_4)$, that is, sets I, II, III, IV, V, VI, VII, and VIII, the transmittance phases (values of ψ) become $0^\circ, 45^\circ,$

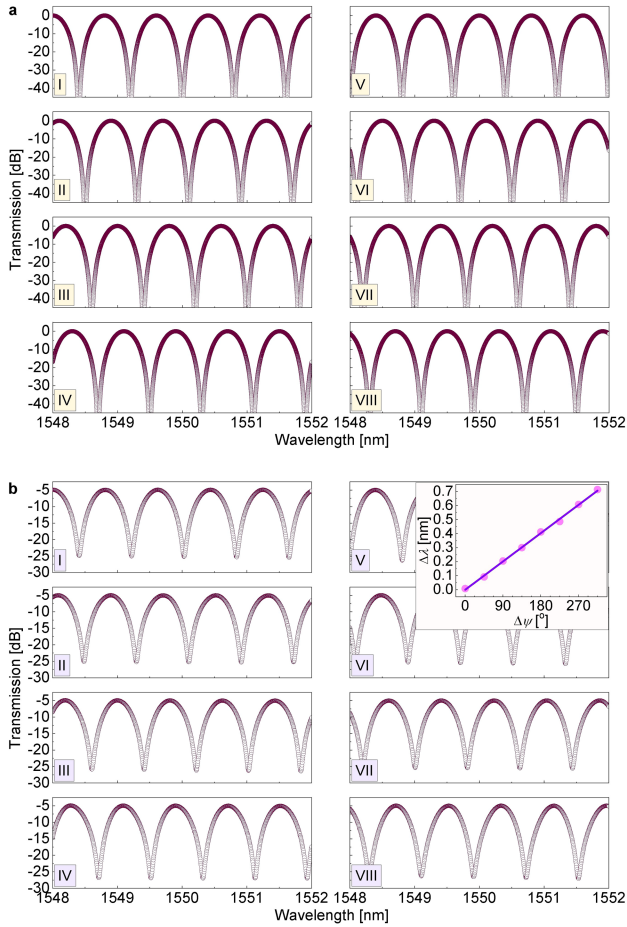


Fig. 4. (a) Calculated narrowband comb spectra for theoretical QWP AA sets I–VIII chosen from Fig. 3 with θ_{P1} set to 0° and (b) measured narrowband comb spectra of constructed filter for experimental QWP AA sets I–VIII shown in Table I.

90° , 135° , 180° , 225° , 270° , and 315° , respectively. This implies that the narrowband comb spectrum at set I is wavelength-tuned by $\lambda_{FSR}/8$, $\lambda_{FSR}/4$, $3\lambda_{FSR}/8$, $\lambda_{FSR}/2$, $5\lambda_{FSR}/8$, $3\lambda_{FSR}/4$, and $7\lambda_{FSR}/8$ at sets II, III, IV, V, VI, VII, and VIII, respectively. This stepwise wavelength tuning can readily be extended to continuous wavelength tuning by carefully choosing the QWP AA sets of $(\theta_1, \theta_2, \theta_3, \theta_4)$ such that ψ varies from 0° to 360° along the parametric curves in Fig. 3(b) and (d).

III. WAVELENGTH-TUNED NARROWBAND COMB SPECTRA

In order to validate the spectral shift of the proposed filter, which varies according to the QWP AA set, the filter transmission spectrum was calculated for the chosen AA sets mentioned above, i.e., sets I–VIII. Fig. 4(a) shows eight narrowband comb spectra calculated for sets I–VIII with θ_{P1} set to 0° at a wavelength range from 1548 to 1552 nm. Because the birefringence B of the PMF to be used in the fabrication of the proposed filter was measured to be 4.166×10^{-4} , the length L of each PMF segment was determined to be 7.2 m to make $\lambda_{FSR} \sim 0.8$ nm. As with the t_f derivation, the spectrum calculation also assumes that the insertion losses of all optical components within the

filter are zero and that the phase retardation differences of all QWPs are independent of wavelength over a wavelength range of interest. The figure illustrates that as the set number increases, the narrowband comb spectrum shifts to longer wavelengths. When the AA set changes from set I to set II, the first transmission minimum at set I, located at 1548.4 nm, shifts by $\lambda_{FSR}/8$ (≈ 0.1 nm) to a longer wavelength region. This red shift of $\lambda_{FSR}/8$ occurs with each set change as the set number increases from I to VIII. Moreover, spectral calculations were carried out even for other AA sets besides the eight selected AA sets, which can be picked out from the curves of Fig. 2 or Fig. 3. From these spectral calculations, we could confirm that a change in the AA set causing 1° increase in ψ leads to a red shift of $\lambda_{FSR}/360$ in the narrowband comb spectrum. The above calculation results support the continuous wavelength shift of the narrowband comb spectrum in the proposed filter. Therefore, this theoretical analysis predicts that our filter, which harnesses the all-quarter-wave polarization transformation, can achieve the continuous wavelength tuning capability by the proper choice of AA sets $(\theta_1, \theta_2, \theta_3, \theta_4)$.

On the other hand, the spectral evolution of the SOP_{out} of PMF 2 determines the transmission spectrum of the proposed filter. Thus, a spectral shift in this transmission spectrum is directly related to a variation in the spectral evolution of the SOP_{out} of PMF 2, which can be induced by controlling the QWP AAs. As the wavelength increases by λ_{FSR} , the evolution of the PMF 2 SOP_{out} forms a unique SOP trace on the Poincare sphere, namely the SOP_{out} trace of PMF 2. Fig. S1 in the Supplementary Information shows the SOP_{out} traces of PMF 2 for ψ values from 1° to 360° (step: 1°), each trace showing the spectral evolution of the PMF 2 SOP_{out} (indicated by green circles) as the wavelength increases from 1548 to 1548.8 nm with a step of 0.01 nm. The blue and red diamonds, slightly larger than the green circles, indicate the SOP_{out} 's obtained at wavelengths of 1548 and 1548.79 nm, respectively, which serve as reference points to identify the evolution direction of the SOP_{out} . Because the two output spectra of the CW and CCW light propagation paths shown in Fig. 1(b) are equivalent except for their insertion losses [25], [26], only the CW path is considered in the analysis of the SOP_{out} traces. Since the light passing through PMF 2 undergoes a linear horizontal polarizer at the PBS, the SOP_{out} of PMF 2 closest to the S1 axis (i.e., LHP) or $-S1$ axis (i.e., LVP) of the Poincare sphere corresponds to the transmission maximum or minimum of the narrowband comb spectrum, respectively. As seen in Fig. S1, the wavelength at which the PMF 2 SOP_{out} lies on the S1 axis varies with ψ . For example, for $\psi = 0^\circ$ (or 360°), the SOP_{out} is on the S1 axis at 1548 nm. If ψ is changed to 45° , the SOP_{out} is now on the S1 axis at 1548.1 nm. This wavelength change of the SOP_{out} on the S1 axis means a change of the transmission maximum wavelength, i.e., a wavelength shift in the narrowband comb spectrum. In consequence, the continuous adjustment of ψ by the appropriate control of the QWP AAs allows the continuous wavelength tuning of the SOP_{out} on the S1 axis, resulting in the continuous wavelength tuning of the narrowband comb spectrum.

To experimentally validate the calculated results, we actually constructed the proposed filter composed of one SMF-pigtailed

TABLE I
QWP AA SETS I–VIII FOR WAVELENGTH TUNING OF NARROWBAND COMB
SPECTRA OF CONSTRUCTED FILTER

| Set | θ_1 | θ_2 | θ_3 | θ_4 | λ_m |
|------|------------|------------|------------|------------|-------------|
| I | 179.5° | 70.5° | 39.0° | 21.0° | 1548.408 nm |
| II | 73.5° | 49.0° | 117.0° | 128.0° | 1548.491 nm |
| III | 73.0° | 72.0° | 120.0° | 126.0° | 1548.604 nm |
| IV | 72.0° | 62.0° | 121.0° | 130.0° | 1548.699 nm |
| V | 168.0° | 47.0° | 93.0° | 70.0° | 1548.811 nm |
| VI | 174.0° | 68.0° | 96.0° | 74.0° | 1548.885 nm |
| VII | 162.0° | 66.0° | 94.0° | 69.0° | 1549.007 nm |
| VIII | 177.0° | 39.0° | 37.0° | 20.0° | 1549.113 nm |

four-port PBS (OZ Optics), two ~ 7.12 m segments of bow-tie type PMF (Fibercore), four SMF-pigtailed QWPs (OZ Optics), as shown in Fig. 1. The slow-axis AAs of all QWPs can be adjusted from 0° to 360° using their control knobs. The length of the PMF segment was determined by considering the PMF birefringence $B (= 4.166 \times 10^{-4})$ to set λ_{FSR} to ~ 0.8 nm at 1550 nm. An amplified spontaneous emission source (Fiberlabs FL7701) and an optical spectrum analyzer (Yokogawa AQ6370C) were employed to measure the output spectrum of the constructed filter. Fig. 4(b) shows the eight narrowband comb spectra of the constructed filter measured for the experimental QWP AA sets I–VIII in Table I at a wavelength range of 1548 to 1552 nm. These spectra were measured with the resolution bandwidth and sensitivity (representing the video bandwidth) of the optical spectrum analyzer set to 0.02 nm and HIGH1, respectively. As seen in the figure, the narrowband comb spectrum showed a red shift of ~ 0.1 nm with each increment of the set number, resulting in a total wavelength shift of ~ 0.7 nm for the AA set change from set I to set VIII, which agrees well with the calculated results. The average insertion loss and extinction ratio of the eight narrowband comb spectra were measured to be ~ 5.05 and ~ 19.9 dB, respectively. In addition, the measured flatness between five passbands was less than 0.11 dB. The inset of Fig. 4(b) shows the wavelength shift of the first transmission minimum in set I, located at 1548.408 nm, as the set number in Table I increases from I to VIII. The absolute wavelength λ_m of the first transmission minimum is suggested for each set in Table I. A burgundy solid line indicates the linear regression result of the measured wavelength data of the first transmission minimum, resulting in an adjusted R^2 value of ~ 0.99823 . This analysis result implies good wavelength tuning linearity for the eight narrowband comb spectra shown in Fig. 4(a). Through additional spectral measurements on other QWP AA sets other than the eight sets in Table I, we also confirmed the wavelength tuning capability of other narrowband comb spectra that exist between comb spectra of any two adjacent ones of the eight sets. As a result, our experimental findings from the constructed filter effectively validate the predicted continuous wavelength-tuning capability of the narrowband comb spectrum in the proposed filter based on the all-quarter-wave polarization transformation. Our wavelength-tunable narrowband PDFL filter is anticipated to make beneficial contributions to optical signal processing in various optical applications, such as microwave and optical

signal processing [29], [4], waveband switching [30], [31], and optical sensor demodulation, not to mention the enhancement of system form factor. In addition, the effect of temperature or pressure on SOP evolution and thus filter performance should not be ignored. A temperature- or pressure-induced change in birefringence or temperature- or pressure-induced microbending of PMF and even SMF can modulate the SOP of light propagating through the optical elements within the filter. For an ambient temperature variation within $1-2^\circ\text{C}$, this temperature-induced effect is negligible, but large temperature changes over 10°C can severely degrade the wavelength-tuning operation of the filter. Similarly, external pressure changes greater than 0.1 MPa can also affect filter operation. Therefore, for the sake of the filter's operational stability, the entire filter device except the input and output fibers can be hermetically sealed to protect the filter from external temperature or pressure disturbances, and even a thermoelectric cooler can be utilized for more robust operation.

REFERENCES

- [1] Q. Li, C.-H. Lin, P.-Y. Tseng, and H. P. Lee, "Demonstration of high extinction ratio modal interference in a two-mode fiber and its applications for all-fiber comb filter and high-temperature sensor," *Opt. Commun.*, vol. 250, pp. 280–285, 2005, doi: [10.1016/j.optcom.2005.02.030](https://doi.org/10.1016/j.optcom.2005.02.030).
- [2] W. Jin, C. Wang, H. Xuan, and W. Jin, "Tunable comb filters and refractive index sensors based on fiber loop mirror with inline high birefringence microfiber," *Opt. Lett.*, vol. 38, pp. 4277–4280, 2013, doi: [10.1364/OL.38.004277](https://doi.org/10.1364/OL.38.004277).
- [3] E. Hamidi, D. E. Leaird, and A. M. Weiner, "Tunable programmable microwave photonic filters based on an optical frequency comb," *IEEE Trans. Microw. Theory Tech.*, vol. 58, no. 11, pp. 3269–3278, Nov. 2010, doi: [10.1109/TMTT.2010.2076970](https://doi.org/10.1109/TMTT.2010.2076970).
- [4] J. Ge and M. P. Fok, "Passband switchable microwave photonic multiband filter," *Sci. Rep.*, vol. 5, 2015, Art. no. 15882, doi: [10.1038/srep15882](https://doi.org/10.1038/srep15882).
- [5] I. K. Hwang, S. H. Yun, and B. Y. Kim, "All-fiber tunable comb filter with nonreciprocal transmission," *IEEE Photon. Technol. Lett.*, vol. 10, no. 10, pp. 1437–1439, Oct. 1998, doi: [10.1109/68.720286](https://doi.org/10.1109/68.720286).
- [6] J. Kim, J. Park, S. Chung, N. Park, B. Lee, and K. Jeong, "Bidirectional wavelength add/drop multiplexer using two separate MUX and DEMUX pairs and reflection-type comb filters," *Opt. Commun.*, vol. 205, pp. 321–327, 2002, doi: [10.1016/S0030-4018\(02\)01387-1](https://doi.org/10.1016/S0030-4018(02)01387-1).
- [7] Z. C. Luo, W. J. Cao, A. P. Luo, and W. C. Xu, "Polarization-independent, multifunctional all-fiber comb filter using variable ratio coupler-based Mach-Zehnder interferometer," *J. Lightw. Technol.*, vol. 30, pp. 1857–1862, Jun. 2012, doi: [10.1109/JLT.2012.2190583](https://doi.org/10.1109/JLT.2012.2190583).
- [8] A. P. Luo, Z. C. Luo, W. C. Xu, and H. Cui, "Wavelength switchable flat-top all-fiber comb filter based on a double-loop Mach-Zehnder interferometer," *Opt. Exp.*, vol. 18, pp. 6056–6063, 2010, doi: [10.1364/OE.18.006056](https://doi.org/10.1364/OE.18.006056).
- [9] A. P. Luo, Z. C. Luo, and W. C. Xu, "Multiwavelength switchable erbium-doped fiber ring laser with a PBS-based Mach-Zehnder comb filter," *IEEE Photon. J.*, vol. 3, no. 2, pp. 197–202, Apr. 2011, doi: [10.1109/JPHOT.2011.2120601](https://doi.org/10.1109/JPHOT.2011.2120601).
- [10] M. Han, X. Li, S. Zhang, H. Han, J. Liu, and Z. Yang, "Tunable and channel spacing precisely controlled comb filters based on the fused taper technology," *Opt. Exp.*, vol. 26, pp. 265–272, 2018, doi: [10.1364/OE.26.000265](https://doi.org/10.1364/OE.26.000265).
- [11] G. Sun, D. S. Moon, A. Lin, W. T. Han, and Y. Chung, "Tunable multiwavelength fiber laser using a comb filter based on erbium-ytterbium co-doped polarization maintaining fiber loop mirror," *Opt. Exp.*, vol. 16, pp. 3652–3658, 2008, doi: [10.1364/OE.16.003652](https://doi.org/10.1364/OE.16.003652).
- [12] O. Pottiez, B. Ibarra-Escamilla, E. A. Kuzin, R. Grajales-Coutino, and A. Gonzalez-Garcia, "Tuneable Sagnac comb filter including two wave retarders," *Opt. Laser Technol.*, vol. 42, pp. 403–408, 2010, doi: [10.1016/j.optlastec.2009.08.008](https://doi.org/10.1016/j.optlastec.2009.08.008).
- [13] Z. X. Zhang, Z. W. Xu, and L. Zhang, "Tunable and switchable dual-wavelength dissipative soliton generation in an all-normal-dispersion Yb-doped fiber laser with birefringence fiber filter," *Opt. Exp.*, vol. 20, pp. 26736–26742, 2012, doi: [10.1364/OE.20.026736](https://doi.org/10.1364/OE.20.026736).

- [14] Y. Chang, L. Pei, T. Ning, J. Zheng, J. Li, and C. Xie, "Switchable and tunable multi-wavelength fiber ring laser employing a cascaded fiber filter," *Opt. Fiber Technol.*, vol. 58, 2020, Art. no. 102240, doi: [10.1016/j.yofte.2020.102240](https://doi.org/10.1016/j.yofte.2020.102240).
- [15] Y. W. Lee, K. J. Han, B. Lee, and J. Jung, "Polarization-independent all-fiber multiwavelength-switchable filter based on a polarization-diversity loop configuration," *Opt. Exp.*, vol. 11, pp. 3359–3364, 2003, doi: [10.1364/OE.11.003359](https://doi.org/10.1364/OE.11.003359).
- [16] Y. W. Lee, K. J. Han, J. Jung, and B. Lee, "Polarization-independent tunable fiber comb filter," *IEEE Photon. Technol. Lett.*, vol. 16, no. 9, pp. 2066–2068, Sep. 2004, doi: [10.1109/LPT.2004.832601](https://doi.org/10.1109/LPT.2004.832601).
- [17] Y. W. Lee, H.-T. Kim, J. Jung, and B. Lee, "Wavelength-switchable flat-top fiber comb filter based on a Solc type birefringence combination," *Opt. Exp.*, vol. 13, pp. 1039–1048, 2005, doi: [10.1364/OPEX.13.001039](https://doi.org/10.1364/OPEX.13.001039).
- [18] Y. W. Lee, H.-T. Kim, and Y. W. Lee, "Second-order all-fiber comb filter based on polarization-diversity loop configuration," *Opt. Exp.*, vol. 16, pp. 3871–3876, 2008, doi: [10.1364/OE.16.003871](https://doi.org/10.1364/OE.16.003871).
- [19] J. Jung and Y. W. Lee, "Tunable fiber comb filter based on simple waveplate combination and polarization-diversified loop," *Opt. Laser Technol.*, vol. 91, pp. 63–70, 2017, doi: [10.1016/j.optlastec.2016.11.026](https://doi.org/10.1016/j.optlastec.2016.11.026).
- [20] J. Jung and Y. W. Lee, "Continuously tunable polarization-independent zeroth-order fiber comb filter based on polarization-diversity loop structure," *Appl. Phys. B*, vol. 123, 2017, Art. no. 106, doi: [10.1007/s00340-017-6697-8](https://doi.org/10.1007/s00340-017-6697-8).
- [21] J. Jung and Y. W. Lee, "Continuously wavelength-tunable passband-flattened fiber comb filter based on polarization-diversified loop structure," *Sci. Rep.*, vol. 7, 2017, Art. no. 8311, doi: [10.1038/s41598-017-06952-z](https://doi.org/10.1038/s41598-017-06952-z).
- [22] J. Jung and Y. W. Lee, "Polarization-independent wavelength-tunable flat-top comb filter based on quarter-wave polarization transformation," *Jpn. J. Appl. Phys.*, vol. 61, 2022, Art. no. 032001, doi: [10.35848/1347-4065/ac4a07](https://doi.org/10.35848/1347-4065/ac4a07).
- [23] J. Jung and Y. W. Lee, "Continuously wavelength-tunable passband-flattened fibre multiwavelength filter based on heterogeneous combination of wave retarders," *Micro Nano Lett.*, vol. 17, pp. 309–318, 2022, doi: [10.1049/mna2.12137](https://doi.org/10.1049/mna2.12137).
- [24] J. Jung and Y. W. Lee, "Polarization-independent wavelength-tunable first-order fiber comb filter," *IEEE Photon. J.*, vol. 11, no. 1, Feb. 2019, Art. no. 7100515, doi: [10.1109/JPHOT.2018.2886264](https://doi.org/10.1109/JPHOT.2018.2886264).
- [25] J. Jung and Y. W. Lee, "Continuously wavelength-tunable first-order narrowband fiber comb filter using composite combination of wave retarders," *Appl. Sci.*, vol. 10, 2020, Art. no. 6150, doi: [10.3390/app10186150](https://doi.org/10.3390/app10186150).
- [26] J. Jung and Y. W. Lee, "Frequency-tunable optical fiber passband-squeezed birefringence filter based on quarter-wave polarization conversion," *Opt. Commun.*, vol. 510, 2022, Art. no. 127909, doi: [10.1016/j.optcom.2022.127909](https://doi.org/10.1016/j.optcom.2022.127909).
- [27] I. Solc, "Birefringent chain filters," *J. Opt. Soc. Amer.*, vol. 55, pp. 621–625, 1965, doi: [10.1364/JOSA.55.000621](https://doi.org/10.1364/JOSA.55.000621).
- [28] R. C. Jones, "A new calculus for the treatment of optical systems I. Description and discussion of the calculus," *J. Opt. Soc. Amer.*, vol. 31, pp. 488–493, 1941, doi: [10.1364/JOSA.31.000488](https://doi.org/10.1364/JOSA.31.000488).
- [29] J. Li et al., "Photonic polarity-switchable ultra-wideband pulse generation using a tunable Sagnac interferometer comb filter," *IEEE Photon. Technol. Lett.*, vol. 20, no. 15, pp. 1320–1322, Aug. 2008, doi: [10.1109/LPT.2008.926944](https://doi.org/10.1109/LPT.2008.926944).
- [30] X. Cao, V. Anand, Y. Xiong, and C. Qiao, "A study of waveband switching with multilayer multigranular optical cross-connects," *IEEE J. Sel. Areas Commun.*, vol. 21, no. 7, pp. 1081–1095, Sep. 2003, doi: [10.1109/JSAC.2003.815907](https://doi.org/10.1109/JSAC.2003.815907).
- [31] L. Guo, X. Wang, J. Cao, W. Hou, and L. Pang, "Multicast grooming algorithm in waveband switching optical networks," *J. Lightw. Technol.*, vol. 28, pp. 2856–2864, 2010, doi: [10.1109/JLT.2010.2068036](https://doi.org/10.1109/JLT.2010.2068036).